ROYAL SOCIETY OPEN SCIENCE

rsos.royalsocietypublishing.org

Research

Article submitted to journal

Supplemental Material for STEP: Interpretable Extraction of underlying Physics with robust Machine Learning

Karim Alaa El-Din, Alessandro Forte, Muhammad Firmansyah Kasim, Francesco Miniati, Sam Vinko

Department of Physics
University of Oxford
Oxford OX1 3PU, UK

Author for correspondence:
Karim Alaa El-Din

THE ROYAL SOCIETY PUBLISHING

A. Convergence Behaviours

All models described in the main text achieved full epoch convergence as indicated in figures A-1 and A-2 below. The training of the CNN estimator took approximately 1 hour for 5,000 epochs while each STEP estimator took 17 minutes for 10,000 epochs on an AMD Ryzen 5 3500u CPU. Note that while the STEP method loss seems to converge significantly before 10,000 epochs (Fig. A-2), further training allows the estimator to capture the fine structure of a given DoS better, and was therefore maintained.

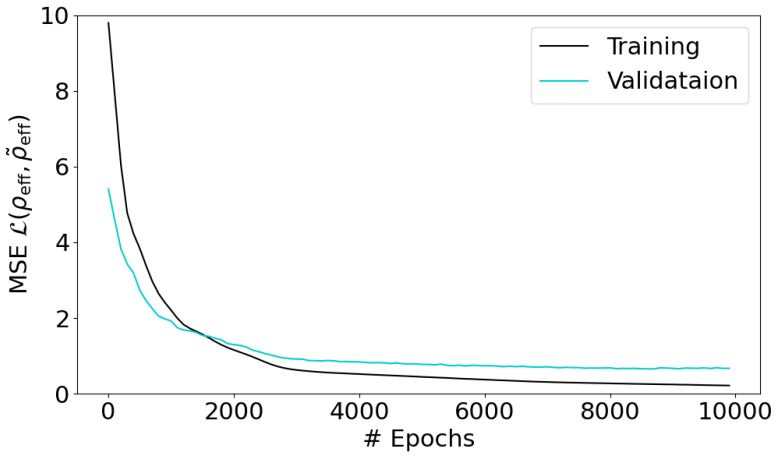

Figure A-1: End-to-end estimator training and validation loss as a function of epochs. The validation consisted of another 45 DoS generated using the same routine as those in the training set. Some overfitting was observed, this worsened significantly for more than 10,000 epochs.

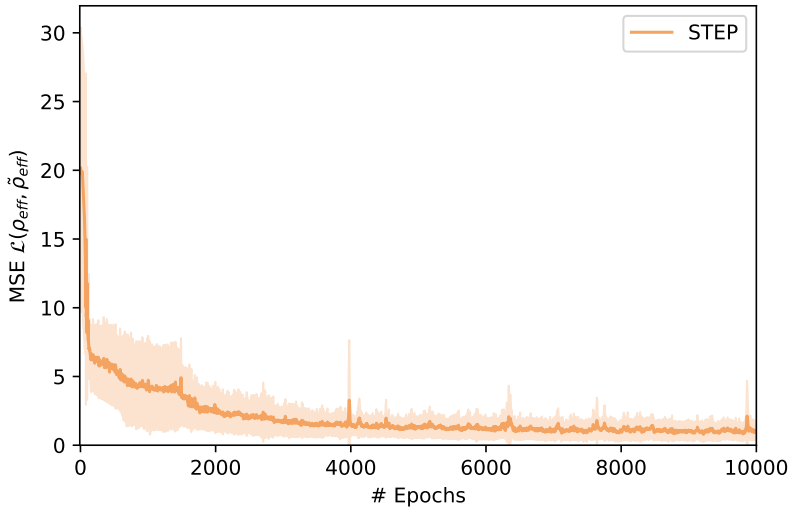

Figure A-2: STEP loss as a function of epochs, averaged over all the 6 DoS, shown with the standard deviation across the different DoS.

B. RIXS Details

B.1 Scattering Theory

An interesting technique for investigations in high energy density science is resonant inelastic X-ray scattering (RIXS) [1,2]. In this process, incoming photons with energy $\hbar\omega_1$ are *inelastically* scattered by a material, yielding photons with a different energy $\hbar\omega_2$ ($\omega_1 \neq \omega_2$). The difference in energy is deposited in the material, specifically in one of its electrons. An illustration of this process can be seen in figure B-1. From now on we set $\hbar = 1$, meaning that the energy of a photon is equivalent to its angular frequency ω.

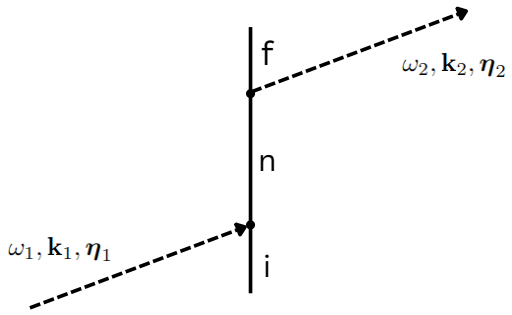

Figure B-1: An illustration of the RIXS scattering, adapted from [2]. The solid black line indicates the state of the probed system, with the labels i, n and f denoting the initial, intermediate and final states respectively. Dashed arrows indicate incoming and outgoing photons, labelled with their energy ω_p, wave vector $\mathbf{k}_p$ and polarization $\boldsymbol{\eta}_p$ for $p = 1, 2$.

The RIXS scattering process can be split, at least conceptually, in an absorption instantaneously followed by an emission: first the incoming photon is absorbed by an inner core electron that is promoted to an excited empty state, then another electron from a different excited state decays filling the vacancy in the core state and emitting the outgoing photon. Both these subprocesses are individually not-energy conserving (the intermediate state n is virtual), but in a way that the overall scattering process conserves energy, as required by general physical laws. It is therefore intuitive from this qualitative description that RIXS allows us to probe the structure of the empty excited states of the system.
The differential cross-section for RIXS [2], proportional to the intensity of scattered radiation measured at energy ω_2 over the whole solid angle, reads in full

$$\partial_{\omega_2}\sigma = 4\pi \left(\frac{e}{m_e c}\right)^4 \frac{\omega_2}{\omega_1}\delta(E_f - E_i + \omega_2 - \omega_1)\left|\sum_n \frac{\langle f|\mathbf{p}(\mathbf{k_2})\cdot\boldsymbol{\eta}_2|n\rangle\langle n|\mathbf{p}(-\mathbf{k_1})\cdot\boldsymbol{\eta}_1|i\rangle}{E_n + i\Gamma_{nf} - E_i - \omega_1}\right|^2. \quad \text{(A 1)}$$

Here, e, m_e, and c take their usual meaning, whereas $|i\rangle$, $|n\rangle$, and $|f\rangle$ indicate initial, intermediate, and final electronic states of the system, with respective energies E_i, E_n and E_f. While the δ function ensures overall energy conservation, the amplitude squared of the sum over intermediate states n depends on the quantum mechanical details of the electronic transitions and its discussion is outside the scope of this work. Suffice it to say that, under reasonable conditions [2,3] we may rewrite this cross-section as

$$\partial_{\omega_2}\sigma = C\frac{\omega_2}{\omega_1}\sum_f \frac{[1 - F_D(\Delta_f; T)]\rho(\Delta_f)A_f|M(\Delta_f)|^2}{[\omega_2 - (\epsilon_f - \epsilon_i)]^2 + \Gamma_f^2}. \quad \text{(A 2)}$$

Here, ϵ_i and ϵ_f are the initial energies of the electron that is excited and of the one that decays, respectively. A_f and Γ_f are physical parameters of the system as defined in [2].
We shall now proceed through the components of this equation one by one and obtain the form of the scattering equations seen in the main text.

(i) We have used $\Delta_f = \omega_1 - \omega_2 + \epsilon_f$ for conciseness.
(ii) $F_D(\Delta_f; T)$ is the Fermi-Dirac distribution at temperature T.
(iii) $\rho(\Delta_f)$ is the electronic density of states of the material under investigation.
(iv) $|M(\Delta_f)|^2$ is the square of the matrix element for a given transition. This term includes quantum effects regulating the probability of different transitions occurring, and therefore regulating their contribution to scattering.
(v) We may now group items (ii), (iii) and (iv) to obtain the *effective* density of states as seen in the main text,

$$\rho_{\text{eff}}(\Delta_f) = [1 - F_D(\Delta_f; T)]\rho(\Delta_f)|M(\Delta_f)|^2. \tag{A 3}$$

This step is necessary, as we have no way of measuring and discerning the individual contributions of these terms. However, if we are able to obtain an independent measurement of T, we can split off the thermal distribution and extract $\rho(\Delta_f)|M(\Delta_f)|^2$.
(vi) The remaining components of the equation now depend solely on the material, its final state f and ω_2. These terms may be regrouped and written as

$$L_f(\omega_2) = C\omega_2 \frac{A_f}{[\omega_2 - (\epsilon_f - \epsilon_i)]^2 + \Gamma_f^2}. \tag{A 4}$$

Finally, we combine all these steps to obtain

$$\partial_{\omega_2}\sigma = \sum_f \frac{L_f(\omega_2)}{\omega_1}\rho_{\text{eff}}(\omega_1 - \omega_2 + \epsilon_f). \tag{A 5}$$

Notice that the Lorentzian factor on L_f suppresses the RIXS signal far from the energy $(\epsilon_f - \epsilon_i)$. This fact, in turn, implies that the reconstruction of ρ_{eff} is unreliable in the regions contributing to the suppressed parts in the RIXS spectra. This can be seen in Fig. 5, where the error bars on the reconstructions increase for $\Delta_f > 100eV$.
The material parameters used for our models can be seen in table B.I.

Parameter[units]	f	Value
$\epsilon_i[eV]$	1, 2	-7112
$\epsilon_f[eV]$	1	-723
	2	-708.5
A_f	1	50
	2	100
$\Gamma_f[eV]$	1	3
	2	2.55

Table B.I: Physical parameters used for the simulations.

B.2 Realistic RIXS Measurements

Note that equation (A 5) only applies to monochromatic light, but that we measure high energy density science RIXS processes using x-ray free electron lasers (XFELs), whose radiation

is generated using self-amplified spontaneous emission (SASE) [4,5]. While useful to probe matter in regimes of interest, SASE pulses generally exhibit broad and highly irregular spectral profiles [6–8] $\Phi_k(\omega_1)$ varying for each shot k, which we need to incorporate into our analysis. To do so, we may first insert a Dirac δ function to write equation (A 5) as

$$\partial_{\omega_2}\sigma = \sum_f L_f(\omega_2) \int_{-\infty}^{\infty} \frac{d\omega_1'}{\omega_1'}\delta(\omega_1 - \omega_1')\rho_{\text{eff}}(\omega_1' - \omega_2 + \epsilon_f). \tag{A 6}$$

Note that this equation now has the characteristic form of a convolution. By replacing $\delta(\omega_1 - \omega_1')$ with our spectral pulse shape $\phi_k(\omega_1')$, and using the weighted pulse shape $\Phi_k(\omega_1') = \phi_k(\omega_1')/\omega_1'$, as well as taking $\omega_1' \to \omega_1$, we obtain

$$\partial_{\omega_2}\sigma_k = \sum_f L_f(\omega_2) \int_{-\infty}^{\infty} d\omega_1 \Phi_k(\omega_1)\rho_{\text{eff}}(\omega_1 - \omega_2 + \epsilon_f), \tag{A 7}$$

exactly as seen in equation (6) of the main text. Note that we have now moved from a description that looked nothing like a convolution to one that obviously corresponds to a convolution with a dynamically varying kernel Φ_k.

C. Estimator Hyperparametrizations

C.1 CNN Hyperparameters

The detailed hyperparameters found for the CNN estimator are listed in table C below.

Hyperparameter	Optimal Value	Space
Optimizer	Adam	Adam
Loss	MSE	MSE, MAE
L2 Regularization	0	0, 1e-5, 5e-5, 1e-4
# conv. Layers	4	1, 2, 3, 4, 5
# conv. Channels	8	2, 4, 8, 16
# FFNN layers	4	1, 2, 4, 8
# Nodes FFNN	(200, 200, 100, 100)	20, 50, 100, 200, or 500 in each layer.

Table C.II: Hyperparameters for the CNN estimator. The # Nodes FFNN parameter is restricted to flat (equal number of nodes) or tapered (decreasing along forward axis) architectures.

C.2 STEP Hyperparametrization

The hyperparameter choice for STEP estimators on the results presented in section **??**(a) was investigated thoroughly and found to have no meaningful impact. Neural network depths between 4 and 10 layers, with 40 to 80 nodes per layer, activation and loss functions were varied with no impact on predictions. However, larger estimators caused significantly longer training times. This led us to use the minimal estimator size, consisting of 4 layers of 40 nodes each. The final estimator was therefore a simple feed-forward neural network with that architecture.

D. Chemical Potential

The chemical potential was calculated using numerical fits of the form

$$\mu/T = \simeq a + b * log(T/E_F) + \frac{c * (T/E_F)^d + e * (T/E_F)^f}{1 + g * (T/E_F)^h}. \quad \text{(A 1)}$$

Here, T is the temperature, E_F is the Fermi energy (calculated through numerical optimzation), and the fit parameters a through h were found using the "curve_fit" function of the SciPy package [9]. For the DoS used in our analysis, they took the values indicated in table D.III below. This fit was used to improve performance of the analysis, as μ would otherwise have to be optimized for at each training epoch.

Parameter	Value
a	0.60944891
b	-0.99060934
c	0.16701814
d	-2.92018411
e	-0.05744572
f	0.70358151
g	0.40826049
h	-1.64569649

Table D.III: Tabulated fit parameters for the chemical potential

E. Data, Code, and Models

All files are available under https://github.com/OxfordHED/rixs_nn_analysis.

References

1. Luuk JP Ament, Michel Van Veenendaal, Thomas P Devereaux, John P Hill, and Jeroen Van Den Brink.
   Resonant inelastic x-ray scattering studies of elementary excitations.
   Reviews of Modern Physics, 83(2):705, 2011.
2. Oliver Humphries.
   Isochoric generation and spectroscopic diagnosis of high energy-density systems.
   PhD thesis, University of Oxford, 2020.
3. OS Humphries, RS Marjoribanks, QY Van Den Berg, EC Galtier, MF Kasim, HJ Lee, AJF Miscampbell, B Nagler, R Royle, JS Wark, et al.
   Probing the electronic structure of warm dense nickel via resonant inelastic x-ray scattering.
   Physical Review Letters, 125(19):195001, 2020.
4. Gianluca Geloni, E Saldin, L Samoylova, E Schneidmiller, H Sinn, Th Tschentscher, and M Yurkov.
   Coherence properties of the european xfel.
   New Journal of Physics, 12(3):035021, 2010.
5. John Arthur.
   Status of the lcls x-ray fel program.
   Review of scientific instruments, 73(3):1393–1395, 2002.
6. Kwang-Je Kim.
   An analysis of self-amplified spontaneous emission.
   Nuclear Instruments and Methods in Physics Research Section A: Accelerators, Spectrometers, Detectors and Associated Equipment, 250(1-2):396–403, 1986.

7. J Andruszkow, B Aune, V Ayvazyan, N Baboi, R Bakker, V Balakin, D Barni, A Bazhan, M Bernard, A Bosotti, et al.
First observation of self-amplified spontaneous emission in a free-electron laser at 109 nm wavelength.
Physical Review Letters, 85(18):3825, 2000.
8. SV Milton, E Gluskin, ND Arnold, C Benson, W Berg, SG Biedron, M Borland, Y-C Chae, RJ Dejus, PK Den Hartog, et al.
Exponential gain and saturation of a self-amplified spontaneous emission free-electron laser.
Science, 292(5524):2037–2041, 2001.
9. Pauli Virtanen, Ralf Gommers, Travis E. Oliphant, Matt Haberland, Tyler Reddy, David Cournapeau, Evgeni Burovski, Pearu Peterson, Warren Weckesser, Jonathan Bright, Stéfan J. van der Walt, Matthew Brett, Joshua Wilson, K. Jarrod Millman, Nikolay Mayorov, Andrew R. J. Nelson, Eric Jones, Robert Kern, Eric Larson, C J Carey, İlhan Polat, Yu Feng, Eric W. Moore, Jake VanderPlas, Denis Laxalde, Josef Perktold, Robert Cimrman, Ian Henriksen, E. A. Quintero, Charles R. Harris, Anne M. Archibald, Antônio H. Ribeiro, Fabian Pedregosa, Paul van Mulbregt, and SciPy 1.0 Contributors.
SciPy 1.0: Fundamental Algorithms for Scientific Computing in Python.
Nature Methods, 17:261–272, 2020.